Development and radiation characteristic evaluation of Advanced Radiation Resistant Austenitic Alloys (AR^2A^2) for reactor internals

Ji Ho Shin, Ho-Sub Kim, Byeong Seo Kong, Hyeon Bae Lee, Changheui Jang*
Dept. of Nuclear and Quantum Engineering, KAIST, Daejeon, Rep. of Korea
**Corresponding Author: chjang@kaist.ac.kr*

1. Introduction

Austenitic stainless steels (ASSs) have been used extensively for nuclear power reactors for many years, because the materials show good mechanical properties. In general, they have shown excellent performance in the environment of high temperature water and neutron irradiation. Nonetheless, as nuclear power plants age and neutron fluence increases, detrimental effects resulting from radiation damage have become an increasingly important issue for the operational safety and structural integrity of internal components. Due to this crucial role, radiation damage and irradiation effects are a critical issue for safety regulation and aging management of LWRs. Thus, it is necessary to develop the radiation resistant austenitic alloy for reactor internals.

Fine precipitates have been known to act as efficient traps or sinks for void or interstitial atoms created by neutron irradiation in the various alloys [1, 2]. In addition, the use of other defect sinks, such as grain boundaries and dislocations could lead to even greater improvement in radiation resistance [3, 4].

In this study, to elucidate the effect of minor alloying element on forming the fine and highly dense precipitate, model alloys based on high chromium stainless steel were fabricated with varying Ti and N contents. Then, by controlling the thermo-mechanical processing condition, we explored how the heat treatment temperature and time influence the microstructure, especially the formation of the fine niobium carbide (NbC). Microstructural analyses were performed particularly focusing on the precipitate size and number density. Finally, their contributions to the radiation resistance properties were estimated.

2. Methods and Results

2.1 Material fabrication and analysis methods

Three heats advanced radiation resistant austenitic alloys (AR^2A^2) were fabricated by vacuum induction melting (VIM) method based on the chemical compositions. The cast alloys were subsequently subjected to various thermo-mechanical processes to produce plates. Then, the plates were machined into rectangular-type specimens of 12 mm (L) x 10 mm (W) x 8 mm (t). Microstructural characteristics of prior austenite grains were examined by etching the surface of test sample with etchant (a hydrochloric acid, bromine + methanol solution). Various analysis techniques such as optical microscope (OM), X-ray diffraction (XRD), scanning electron microscope (SEM) and transmission electron microscope (TEM) were utilized to characterize the microstructure. To identify the morphology, size distribution and number density of precipitates, TEM operating at 200 keV was used. For TEM specimen preparation, three-millimeter discs were cut and electro-polished on a twin jet polisher, using a solution of 90 % methanol and 10 % perchloric acid. Tensile tests were conducted using an instron 8501 machine at room-temperature, 320 ℃ and a strain rate of 5×10^{-4} s^{-1} following the procedures of ASTM E8/E8M [5]. Test samples with their longitudinal axis aligned parallel to the rolling direction were machined in accordance with ASTM standard E466 [6]; the gauge section of the test sample was 24 mm x 6 mm x 1 mm (length x width x thickness).

2.2 Alloy design

One of the most effective precipitates in pinning the grain boundaries is titanium nitride (TiN). Compared with the nitrides of Al, Nb, or V, TiN is known to have a higher thermodynamic stability, i.e., low solubility in the matrix and high resistance to particle coarsening [7, 8]. In order to pin the grain boundaries more effectively, it is emphasized that the TiN precipitate distribution should have the largest volume fraction and smallest particle size possible. However, according to recent researches [9, 10], a high Ti content promotes the formation of coarse TiN particles with sizes over 0.5 μm. These particles are ineffective in pinning the grain boundaries and can act as cleavage nucleation sites. Therefore, the control of Ti contents is important in order to maintain fine particles for inhibiting grain growth whilst avoiding the possibility of coarse particles that may impair toughness. Furthermore, in order to improve the IASCC resistance of stainless steel, the stainless steels are stabilized with fine and well distributed TiN as well as NbC precipitates which act as sink site. A few studies had been carried out [11-14] to evaluate the effects of nitride and carbide precipitates on RIS and swelling behaviour in irradiated austenitic stainless steel. The void swelling in Ti-modified 316 stainless steel had been studied. The results had indicated that the swelling observed in Ti-modified 316 stainless steel is much smaller than that in standard 316 stainless steel [11]. Another study had reported that the RIS in high purity type 347 stainless steel, chromium

depletion did not occur at grain boundaries [12]. The other study [13] had reported that a fine dispersion of titanium carbide within the matrix in type 321 stainless steel was effective in suppressing void swelling. However, this was correlated to the stability of titanium carbide. The reduced stability of titanium carbide with irradiation was one of the reasons of higher void swelling at higher doses [13, 14]. Moreover, higher Cr content that is beneficial to corrosion resistance are used.

Three heats of AR^{2}A^2 with a similar nominal composition, except for Ti and N additions, were used in this study and the chemical composition analyzed by inductively coupled plasma (ICP) method is shown in Table 1. The property diagram and amount of Ti-rich phase has been calculated using Thermo-Calc (Fig. 1). The fine TiN precipitates were analyzed by TEM/EDS according to Ti/N ratio (Fig. 2). The size of the precipitates becomes smaller as the ratio increases. The results are summarized in the bar graph and table (Fig. 3, Table 2).

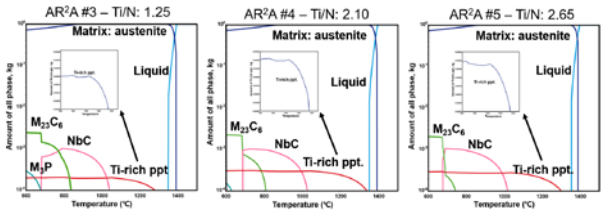

Fig. 1. Property diagrams of AR^{2}A^2 #3, #4 and #5 conducted by Thermo-Calc.

Table 1
Chemical composition of AR^{2}A^2 (in wt. %)

	Fe	Cr	Ni	C	Mn	Si	Nb	Ti	N
AR^{2}A^2 #3	Bal.	24.3	20.9	0.014	1.5	1.25	0.1	0.015	0.012
AR^{2}A^2 #4	Bal.	24.0	21.2	0.013	1.5	1.27	0.1	0.023	0.011
AR^{2}A^2 #5	Bal.	23.7	21.1	0.012	1.5	1.25	0.1	0.022	0.008

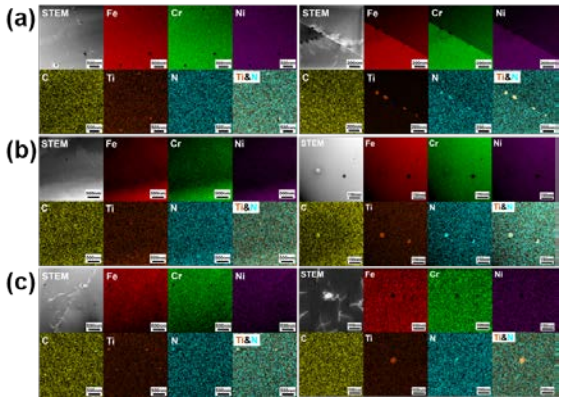

Fig. 2. TEM/EDS mapping micrographs of TiN precipitates for (a) AR^{2}A^2 #3, (b) #4 and (c) #5

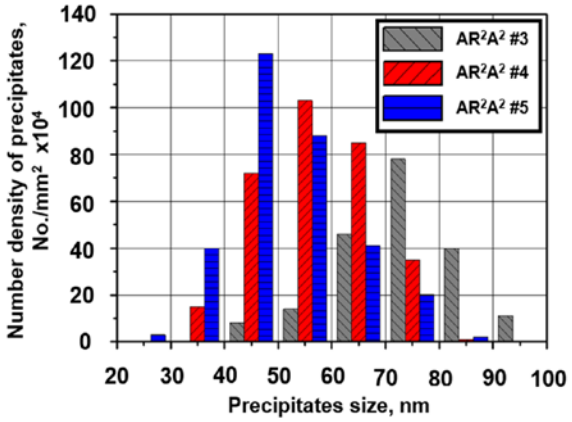

Fig. 3. Size distribution of TiN precipitates number density in the base plates of the three heats

Table 2
Fine TiN precipitates mean size and number density in AR^{2}A^2 #3, #4 and #5

Heats	Measured features	Base plate
AR^{2}A^2 #3	Mean size, nm	72
(Ti/N: 1.25)	Number density, /mm^2	19.7 x 10^5
AR^{2}A^2 #4	Mean size, nm	24.0
(Ti/N: 2.10)	Number density, /mm^2	31.1 x 10^5
AR^{2}A^2 #5	Mean size, nm	23.7
(Ti/N: 2.65)	Number density, /mm^2	31.7 x 10^5

2.3 Thermo-mechanical processing

All alloys developed were first subjected to homogenization heat treatment at 1250 ℃ for 3 h. Subsequently, rolling process was conducted which was composed of seven passes to achieve a total thickness reduction of 80% (thickness reduction of 20% per pass). After completing the rolling process, the alloys were quenched to room temperature with a cooling rate of 20 ℃/s and solution annealed at 1050 ℃ for 1 h. Then, the solution-treated specimens were subjected to cold rolling at 30 % and heat treated at 1000 ℃ for 30 minutes. This was to form dislocations inside the matrix, which would act as nucleation sites for fine NbC. It is known that the well-developed dislocation structure inside austenite grain promotes the precipitation kinetics through pipe diffusion along the dislocation core [15, 16]. Finally, for formation of fine NbC, the alloys were heat-treated at 850 ℃ for 0.5 - 4 h. This temperature was selected considering the result of Thermo-Calc simulation and ASME B&PVC Sec. II, Part A, SA-312.

The TEM micrographs showing the precipitation characteristics of the alloys with different TMP processes are presented in Fig. 4. All precipitates had a spherical shape and their chemical compositions were Nb and C. Precipitates were identified as mostly NbC carbides. It is noted that the precipitation characteristics including the size and distribution of carbides were significantly affected by the heat treatment condition. The size and distribution of precipitate phase at 850 ℃

for 0.5, 1, 2 and 4 hour heat treatment are summarized in the bar graph and shown in Fig. 5 and numerically summarized in Table 3. The size of carbide was not significantly different with the heat treatment time but it increased with time and saturated at 4 hours.

Fig. 6 shows tensile test results at room temperature (25 ℃) and high temperature (320 ℃). The tensile test subjected to type 316 stainless steel, AR^2A^2 #5 (30 % CW + HT (1000 ℃/30 min), 30 % CW + HT (1000 ℃ /30 min + 850 ℃/4 hr)). Due to the fine precipitates as following the TMP process, yield strength and tensile strength increase and elongation decreases. Comparing this result with the mechanical properties of commercial 316 stainless steel, it is considered sufficient to use the AR^2A^2 material as reactor internal structure.

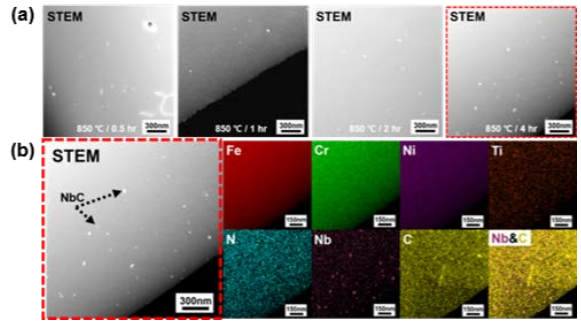

Fig. 4. (a) TEM micrographs of the spherical NbC in aged at 850 ℃ for 0.5, 1, 2 and 4 h and (b) TEM/EDS mapping micrographs of NbC carbide after aging at 850 ℃ for 4h (AR^2A^2 #5)

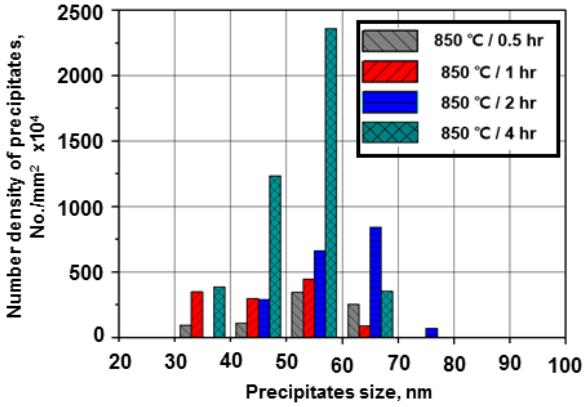

Fig. 5. Size distribution of NbC in aged at 850 ℃ for 0.5, 1, 2 and 4 h (AR^2A^2 #5)

Table 3
Fine TiN precipitates mean size and number density (AR^2A^2 #5)

HT conditions	Measured features	Base plate
Temp.: 850 ℃	Mean size, nm	29.7
Time: 0.5 h	Number density, /mm^2	782 x 10^5
Temp.: 850 ℃	Mean size, nm	26.2
Time: 1 h	Number density, /mm^2	1,179 x 10^5
Temp.: 850 ℃	Mean size, nm	31.5
Time: 2 h	Number density, mm^2	1,794 x 10^5
Temp.: 850 ℃	Mean size, nm	28.1
Time: 4 h	Number density, /mm^2	4,330 x 10^5

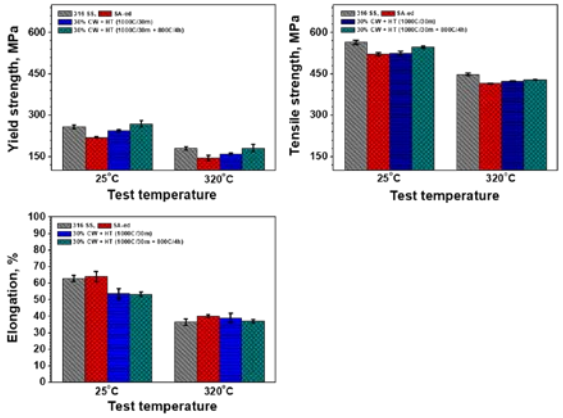

Fig. 6. Tensile test results of 316 SS and AR^2A #5 at room temperature and 320 ℃.

2.4 Sink strength

Fig. 7 summarizes the effect of initial point defect sink strength on radiation hardening observed in several ferrite/martensitic steels irradiated with fission neutrons near 300 ℃ [17] and sink strength of reference alloys such as 304L SS, UFG 304L SS, TP 347H SS, D9 [18-20] and AR^2A^2. The sink strength was calculated from microstructural data obtained from the unirradiated samples using standard kinetic rate theory expressions [21, 22]. Compared with FMS, ODS and UFG SS, the sink strength of AR^2A^2 alloys show lower value, but is much greater than austenitic stainless steels currently used in LWRs. Also, it is difficult to apply ODS and UFG SS manufacturing process and FMS does not have sufficient corrosion resistance for use as LWR reactor internal structures. Therefore, in comparison to such radiation resistant materials, it can be said that AR^2A^2 has a reasonably high sink strength and much better corrosion resistance. Currently, further improvement in sink strength is pursued by refining the TiN precipitates.

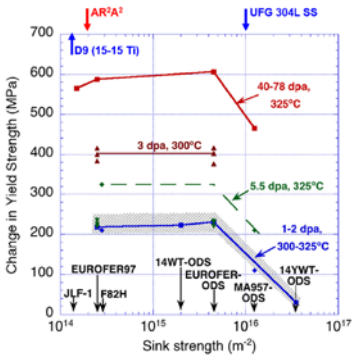

Fig. 7. Effect of initial sink strength on the low temperature radiation hardening behavior of fission reactor irradiated ferritic / martensitic steels [17] and reference alloys [18-20]

3. Summary

The AR^2A^2 alloys were developed as reactor internal materials with superior radiation resistance. In setting the chemical composition, the matrix was made fully austenitic stainless steel and fine precipitation was formed by the subsequent heat treatment. An optimum Ti/N ratio was selected by analyzing the fraction and size of precipitation phase. In addition, Cr content was kept high for superior SCC and IASCC resistance. NbC could be selectively obtained by setting appropriate temperature and time for TMP. Evaluation of radiation characteristics by sink strength calculations shows that AR^2A^2 has a reasonably high value. Further alloy design and TMP optimization will be conducted to obtain a finer and high number density of precipitates in the matrix for higher sink strength values needed for LWR internal materials. We will also carry out the evaluation of the susceptibility to radiation induced degradation such as RIS, radiation embrittlement and IASCC by carrying out the ion irradiation on the developed material.

REFERENCES

[1] F.A. Garner et al., Irradiation performance of cladding and structural steels in liquid metal reactors, Materials science and technology, Vol. 10A, pp. 419, 1994.
[2] E.H. Lee et al., A mechanism of swelling suppression in phosphorous-modified Fe-Ni-Cr alloys, Journal of Nuclear Material, Vol. 695, pp. 141–143, 1986.
[3] H. Kurishita et al., Development of Mo alloys with improved resistance to embrittlement by recrystallization and irradiation, Journal of Nuclear Material, Vol. 233, pp. 557–564, 1996.
[4] Y. Kitsunai et al., Effect of neutron irradiation on impact properties of TiC-dispersed molybdenum alloys, Journal of Nuclear Material, Vol. 239, pp. 253–260, 1996.
[5] ASTM Standard E8-8M, Standard test methods for tension testing of metallic materials, ASTM international, 2013.
[6] ASTM Standard E466-82, Practice for Conducting Constant Amplitude Axial Fatigue Tests of Metallic Materials, ASTM international, 1987.
[7] J. Strid et al., On the chemistry and stability of complex carbides and nitrides in microalloyed steels, Acta Metallurgica, Vol. 33, pp. 2059, 1985.
[8] S. Suzuki et al., The response of carbo-nitride particles in hsla steels to weld thermal cycles, Acta Metallurgica, Vol. 35, pp. 341-352, 1987.
[9] M.A. Linaza et al., Cleavage fracture of microalloyed forging steels, Scripta Metallurgica, Vol. 32, pp. 395-400, 1995.
[10] M.A. Linaza et al., Influence of the microstructure on the fracture toughness and fracture mechanisms of forging steels microalloyed with titanium with ferrite-pearlite structures, Scripta Metallurgica, Vol. 29, pp. 451-456, 1993.
[11] J. Sun et al., Electron irradiation damage in austenitic stainless steels, Journal of Nuclear Materials, Vol. 179-181, pp. 526-528, 1991.
[12] T. Fukuda et al., Microstructural changes of austenitic steels caused by proton irradiation under various conditions, Journal of Nuclear Materials, Vol. 283-287, pp. 263-267, 2000.
[13] T. Kimoto et al., Void swelling and precipitation in a titanium-modified austenitic stainless steel under proton irradiation, Journal of Nuclear Materials, Vol. 132, pp. 266-276, 1985.
[14] R.M. Boothby et al., The effects of silicon and titanium on void swelling and phase transformations in neutron irradiated 12Cr-15Ni steels, Journal of Nuclear Materials, Vol. 152, pp. 123-138, 1988.
[15] P.M. Scott et al., An Analysis of Baffle/Former Bolt Cracking in French PWRs, ASTM STP, Vol 1401, pp. 210-223, 2010.
[16] P.J. Maziasz et al., Microstructural Evolution in Annealed Austenitic Steels during Neutron Irradiation, International Materials Reviews, Vol. 32, pp. 190-219, 1987.
[17] S.J. Zinkle et al., Development of next generation tempered and ODS reduced activation ferritc/martensitic steels for fusion energy applications, Nuclear Fusion, Vol. 57, pp. 17, 2017.
[18] C. Sun et al., Superior radiation-resistant nanoengineered austenitic 304L stainless steel for applications in extreme radiation environments, Material Science Engineering, Vol. 5, pp. 7801, 2015.
[19] K. Yoshikawa et al., Fabrication and properties of corrosion resistant TP347H stainless steel, Journal of Materials Engineering and Performance, Vol. 10, pp. 69-84, 1988.
[20] S. Balaji et al., Ion irradiation studies on the void swelling behavior of a titanium modified D9 alloy, Journal of Nuclear Materials, Vol. 167. pp. 368-372, 2015.
[21] D.R. Olander et al., Fundamental aspects of nuclear reactor fuel elements, TID-26711-P1, 1976.
[22] A.D. Brailsford et al., The rate theory of swelling due to void growth in irradiated metals, Journal of nuclear material, Vol. 44, pp. 121-135, 1972.